APL Photonics

RESEARCH ARTICLE | JANUARY 02 2024

Phase change plasmonic metasurface for dynamic thermal emission modulation

Special Collection: Photonic Structures for Efficient Thermal Management

Zexiao Wang ; Lin Jing ; Xiu Liu; Xiao Luo ; Hyeong Seok Yun ; Zhuo Li ; Sheng Shen

APL Photonics 9, 010801 (2024)
https://doi.org/10.1063/5.0165663

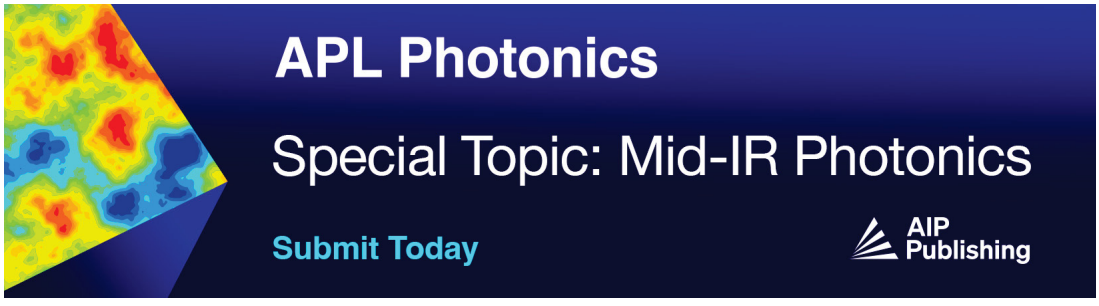

Phase change plasmonic metasurface for dynamic thermal emission modulation

Cite as: APL Photon. 9, 010801 (2024); doi: 10.1063/5.0165663
Submitted: 29 June 2023 • Accepted: 7 December 2023 •
Published Online: 2 January 2024

Zexiao Wang, Lin Jing, Xiu Liu, Xiao Luo, Hyeong Seok Yun, Zhuo Li, and Sheng Shen[a)]

AFFILIATIONS

Department of Mechanical Engineering, Carnegie Mellon University, 5000 Forbes Avenue, Pittsburgh, Pennsylvania 15213, USA

Note: This paper is part of the APL Photonics Special Topic on Photonic Structures for Efficient Thermal Management.
[a)]**Author to whom correspondence should be addressed:** shengshe@andrew.cmu.edu

ABSTRACT

Plasmonic metasurfaces with adjustable optical responses can be achieved through phase change materials (PCMs) with high optical contrast. However, the on–off behavior of the phase change process results in the binary response of photonic devices, limiting the applications to the two-stage modulation. In this work, we propose a reconfigurable metasurface emitter based on a gold nanorod array on a VO_2 thin film for achieving continuously tunable narrowband thermal emission. The electrode line connecting the center of each nanorod not only enables emission excitation electrically but also activates the phase transition of VO_2 beneath the array layer due to Joule heating. The change in the dielectric environment due to the VO_2 phase transition results in the modulation of emissivity from the plasmonic metasurfaces. The device performances regarding critical geometrical parameters are analyzed based on a fully coupled electro-thermo-optical finite element model. This new metasurface structure extends the binary nature of PCM based modulations to continuous reconfigurability and provides new possibilities toward smart metasurface emitters, reflectors, and other nanophotonic devices.

Metasurfaces have shown great promise in manipulating electromagnetic waves to realize novel artificial optical responses.[1,2] The plasmonic metasurfaces with narrowband nearly perfect thermal emission overcomes incoherent thermal emission from objects in the infrared range for important applications in infrared imaging,[3] sensing,[4] and energy harvesting.[5,6] Beyond these passive metasurfaces with fixed functions, dynamic control of the optical responses has become increasingly imperative for achieving various responses in holography,[7–9] infrared camouflage,[10,11] and communication systems.[12,13] The optical properties of a metasurface can be tuned through modulating carrier density,[14] temperature,[15] electric field,[16] or mechanical deformation.[17]

Phase-change materials (PCMs), such as $Ge_2Sb_2Te_5$ (GST) and vanadium dioxide (VO_2), offer a compelling platform for achieving reconfiguration owing to their large refractive index contrast across phase transition.[18,19] While GST-mediated reconfigurable metasurface exhibits multispectral absorptivity (emissivity)[20] and active multistate tunability,[21,22] the rapid heating required for GST phase transition using intense and short voltage pulses poses challenges to device fabrication and scalability. In contrast, associated with the transition of crystal structures between rutile and monoclinic, insulator–metal phase transition of VO_2 can easily occur by electrical or thermal control across the critical temperature of ~340 K.[23] In addition, VO_2 offers a more straightforward device design and a much larger modulation depth due to higher permittivity contrast during the transition, compared to other dynamic tuning mechanisms based on electrostatic gating,[24] electro-optical material,[25] or thermo-optical material.[15] VO_2 based metasurfaces have been used to achieve a binary switching functionality for thermal-switchable absorbers,[26] dual-band emitters,[27] and dual-channel storage or memory devices in the terahertz band,[28,29] but only on–off modulations have been achieved due to the bi-stable nature of the phase change process. A VO_2 reconfigurable thermal emitter with continuous modulation capability remains largely unexplored. Furthermore, the comprehensive modeling of electrically excited phase-change metasurfaces, coupling with optical, electrical, and thermal physics, is still elusive, requiring a detailed investigation on the coupling between microscopic phase change process and device level optical response.

Here, we design a VO_2 based mid-infrared metasurface emitter with continuous reconfigurability and high optical response contrast. The metasurface consists of nanorods with interconnected

electrodes that are used for the phase transition of the underneath VO_2 film by Joule heating. The phase-changing volume of VO_2 (the volume associated with VO_2 that has been phase-changed) can be controlled by a voltage pulse, resulting in continuous emissivity modulation. A fully coupled electro-thermo-optical model is established through the finite element method (FEM) to analyze the continuous evolution of metasurface emissivity with increasing heating voltage. We further investigate the influence of geometrical parameters on the overall optical response. The proposed structure shows great potential in gas sensing[30] and spectroscopy[31] applications as a tunable narrowband mid-infrared emitter, and the continuous tunability on emissivity also makes it a good candidate for display pixels in covert infrared imaging[32] and thermal camouflage[23,33–35] systems. Furthermore, the analysis proves the capability of the proposed structure in extending the well-known binary nature of the PCM modulation, paving a way for reconfigurable nanophotonic devices.

Figure 1 shows the conceptual schematic and basic working principle of the proposed reconfigurable metasurface emitter. As illustrated in Fig. 1(a), the metasurface is designed as a metal–insulator–metal (MIM) structure, consisting of a gold nanorod array as emitting resonators, a VO_2 layer as a spacer, and a thick layer of gold film as a mirror. The phase transition of the VO_2 layer provides a refractive index contrast, resulting in the reconfigurability of the optical response. In addition, a thin Al_2O_3 layer is sandwiched between the gold nanorod array and the VO_2 film for electrical insulation. The emitter structure is well compatible with the existing nanofabrication approaches.[36,37] A set of feasible fabrication steps is described in the supplementary material. Figure 1(b) shows a single unit of the nanorod array, with the x period of 2.4 μm and the y period of 0.5 μm. The length and width of the gold nanorod are 2 μm and 100 nm, respectively, which generates an emissivity peak at 32 THz. The nanorods are connected by centerlines with the width of 150 nm, which are used for Joule heating to activate the phase change process of the VO_2 film. Figure 1(c) shows the cross-sectional view of the single metasurface unit. Joule heating is applied to the nanorod by passing a current through the center-connected electrode wire, which induces a temperature gradient along the nanorod from the center toward both tips. The input heating power controls the lateral phase transition volume of the VO_2 film, resulting in the modulated optical responses and adjustable emissivity of the metasurface array, as shown in Fig. 1(d).

The thermal and optical responses of the metasurface emitter are numerically investigated through FEM simulations. The nanorod MIM metasurface structure with an array size around $16 \times 16\ \mu m^2$ (7 columns and 31 rows), together with a single crystal silicon substrate carrying the whole structure, is modeled through COMSOL Multiphysics. Joule heating is implemented by an electrical current module with a finite voltage difference U_0 across the two electrodes; the steady state and transient temperature responses are investigated on the whole array. The steady state analysis incorporates a DC voltage input from 0.5 to 0.9 V, while the transient input takes a square pulse voltage source with a duration of 20 μs. The electrical conductivity of the gold heater is 4.5×10^7 S/m.[38] The optical response of the metasurface array is simulated using a frequency domain radio frequency (RF) module, focusing on a single unit at the array center combined with periodic boundary conditions surrounding the unit. Due to the inherently stochastic nature of thermal emission, difficulties arise in directly calculating the collective emission of the whole emitter array.[39] However, according to Kirchhoff's law, for the reciprocal materials, the emissivity is equal to the absorptivity,[40] which can be derived in more straightforward calculations using a plane wave excitation. Based on this, a periodic port is incorporated to provide plane wave stimulation, and the reflectance response is evaluated based on the S-parameter on that port. Details on the simulation setup and phase change modeling of VO_2 are elaborated in the supplementary material. The thermal properties for each material layer and the VO_2 properties across phase change,[41–46] as well as the dielectric functions for each layer,[47–49] are summarized in the supplementary material.

The steady state and transient thermal responses of the metasurface emitter are illustrated in Fig. 2. Figure 2(a) is the top-view temperature profile of the array under the voltage of U_0 = 0.9 V. Due to the relatively long nanorod array and the centerline heating design, the thermal interaction between neighboring heater columns is minimal. Under U_0 = 0.9 V, the center and outmost columns

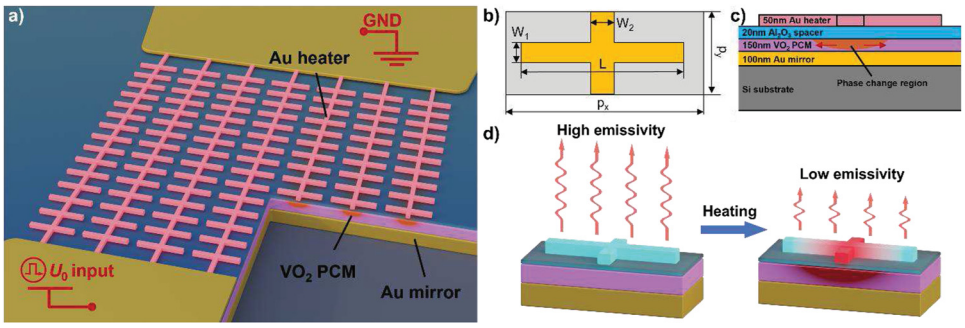

FIG. 1. Device layout of the proposed electrically reconfigurable nanorod metasurface. (a) The schematic of the metasurface structure, which consists of a gold nanorod array placed on the VO_2 phase change material, with another gold layer as the bottom mirror. A thin layer of Al_2O_3 is placed between nanorods and VO_2 as insulation. The nanorod array is connected by centerlines to provide Joule heating. (b) One single unit of the metasurface emitter array with the dimensions of p_x = 2.4 μm, p_y = 0.5 μm, W_1 = 100 nm, W_2 = 150 nm, and L = 2.0 μm. (c) Cross-sectional view of a single unit. Joule heating inside the centerline controls the phase-changed portion of VO_2 PCM. (d) Reconfigurable optical response resulted from the VO_2 phase change, where different phase change portions result in variable coupling between the nanorod and the mirror.

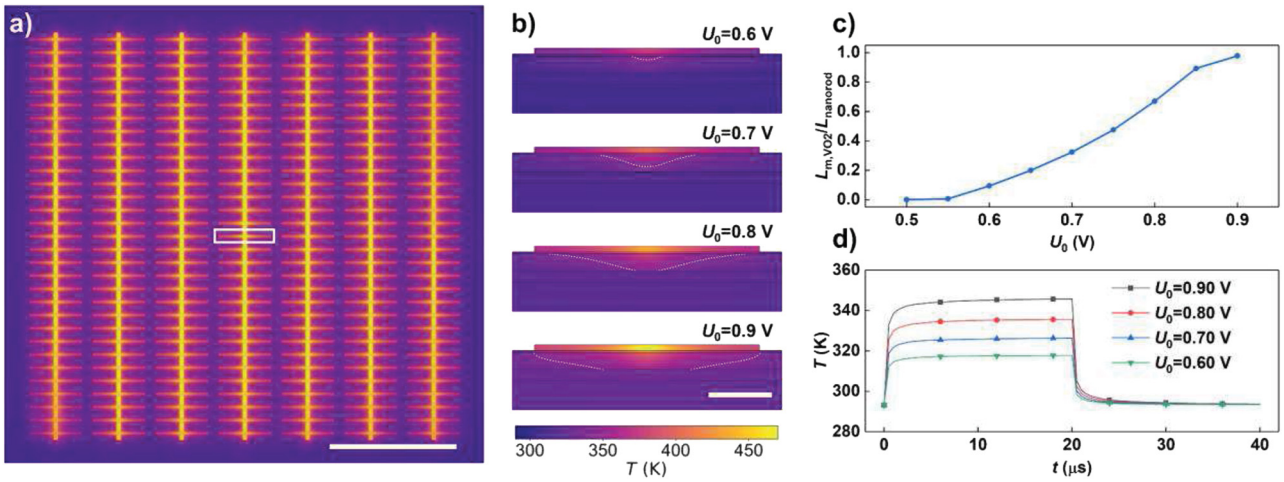

FIG. 2. Steady state and transient thermal response of the Joule heated Au nanorod array. (a) Top-view steady state temperature profile for the array with 7 columns and 31 rows under 0.9 V Joule heating; the scale bar corresponds to 5 μm. (b) Steady state temperature profile and VO_2 phase change interface (white line) for the central unit [white rectangle in (a)] under four different heating voltages. The scale bar corresponds to 500 nm. (c) Length ratio of the phase-changed metal–VO_2 and the full-length of nanorod vs heating voltage. (d) Transient response of the average temperature in the VO_2 region under different heating voltages. The thermal response time is at 5 μs scale.

show a maximum temperature of 481.1 and 471.3 K, respectively, showing largely preserved temperature uniformity (compared to the temperature increase of 180 K). However, within each nanorod unit, a non-negligible local temperature gradient is observed from the centerline to the nanorod tips. Figure 2(a) indicates a temperature difference as large as 85 °C across the whole length of the center nanorod, which can continuously modulate the phase change interface along the nanorod direction under different heating voltages and, thus, the optical responses. The phase change interface evolution can be clearly observed in Fig. 2(b), where the cross-sectional temperature profile of a single unit along the nanorod direction is plotted together with the location of the interface of the phase transition inside the VO_2 layer (white dashed lines). The phase transition interface is estimated based on the phase-change temperature of VO_2 in the heating process. Due to the hysteresis of VO_2, there will be a slight shift in the interface during the cooling process, which is further discussed in the supplementary material. Under a relatively low heating voltage of U_0 = 0.6 V, only a very small portion of the VO_2 film beneath the centerline experiences the phase transition. With increasing the voltage, the gold nanorod effectively spreads the heat along the longitudinal direction, pushing the interface toward the two tips. Under a high voltage of U_0 = 0.9 V, the phase-changed region completely covers the whole length of the nanorod. The change in the dielectric environment of the metasurface will significantly affect the emissivity. Figure 2(c) plots the length ratio between the phase-changed region and the nanorod full length, under different heating voltages. It clearly depicts a steady and continuous increase in the length ratio from 0 to 1 as the heating voltage increases from 0.5 to 0.9 V. Here, through the manipulation of the phase-changed ratio along the nanorod, continuity can be achieved on the VO_2 film beyond intrinsically binary states. The temperature gradient also generates thermal stress inside the device. The device durability under thermally induced stress is discussed in the supplementary material.

We investigate the transient thermal response of the metasurface emitter as the response time is dominated by the thermal time constant in a thermal based reconfigurable optical device.[50] The evolution of emitter maximum temperature with time is plotted in Fig. 2(d) under the square voltage pulses with a duration of 20 μs and different amplitudes applied onto the nanorod array structure. For all the four voltages, no matter whether phase change happens extensively, the emitter reaches the steady state in less than 5 μs, indicating the response time approaching the microsecond level. Here, the transient analysis is based on the whole array simulation, and the thermal mass of the metasurface is highly correlated with the array size. Reducing the array size enables a faster modulation response but causes the diminished optical response.[51] The high thermal conductivity of the substrate is also beneficial for increased modulation speed, while an increased power consumption is required to reach the designed steady state temperature. It is also noted that latent heat does not impose a large influence on the transient thermal response due to the relatively small amount of VO_2, which provides some design freedom in manipulating the thickness of the VO_2 layer for an optimized optical response.

The optical response of the VO_2 based reconfigurable metasurface emitter is shown in Fig. 3. The optical behavior of a single nanorod emitter unit is simulated under a plane wave incident from the top with an electric field parallel along the nanorod direction (TE wave). According to the investigation of the gold nanorod array size in our previous work,[51] the metasurface emitter can be regarded as an infinite large array, and the periodic boundary condition around a single unit is sufficient to simulate the whole array. Different dielectric properties corresponding to metallic and insulating phases of the VO_2 film are assigned based on the thermal simulation of the phase change regions, resulting in voltage-dependent optical responses. Figure 3(a) plots the metasurface emissivity spectrum evaluated based on Kirchhoff's law under different heating voltages. Phase transition does not occur until the voltage reaches 0.6 V, keeping

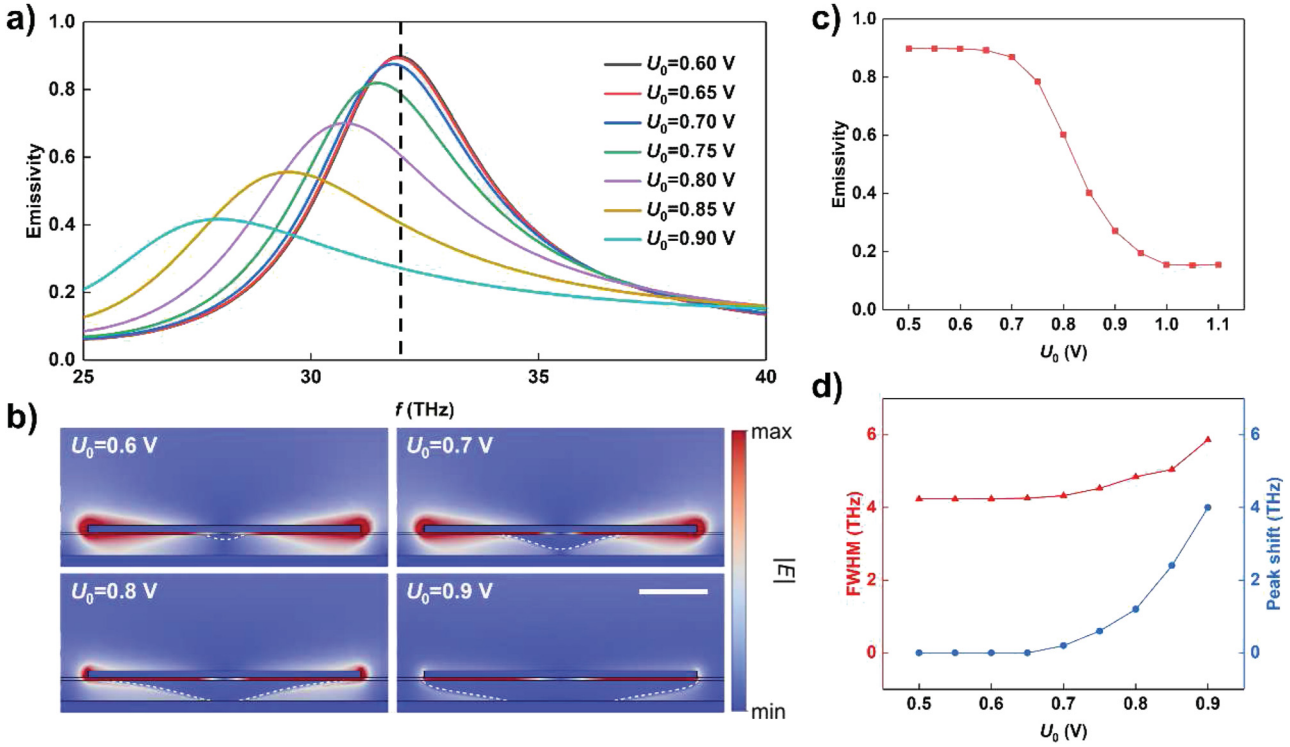

FIG. 3. Simulated optical response of the nanorod metasurface. (a) Emissivity spectrum of the nanorod metasurface under different heating voltages. The maximum emissivity peak is observed at 32 THz for no phase change case, labeled by the black dashed line. (b) Cross-sectional view of the electric field amplitude at four representative heating voltages. The scale bar corresponds to 500 nm. (c) Evolution of emissivity with respect to heating voltages, evaluated at a zero voltage resonance frequency of 32 THz. (d) Evolution of peak shift and FWHM with respect to different heating voltages.

the emissivity peak higher than 0.9 at 32.0 THz (marked as the black dashed line). With a higher heating voltage, the peak becomes more flattened and slightly redshifted due to the insulator–metal transition of the VO_2 film.

The cross-sectional electric field profiles at the emissivity peak frequencies are plotted under different heating voltages in Fig. 3(b). The gold nanorod supports localized plasmonic modes, which behave as electric dipoles under incoming excitation.[14,36] With a relatively low voltage up to $U_0 = 0.6$ V, the VO_2 layer remains mainly at the insulating state. The structure works as a metal–insulator–metal metasurface supporting gap-surface plasmons (GSPs). The scattered thermal radiation from this GSP resonator can be well approximated by the sum of an electric dipole and a magnetic dipole under the multipole expansion.[52,53] Perfect absorption, i.e., zero scattered, thermal radiation occurs when the field completely destructively interferes at the resonance. In other words, the magnetic and electric dipoles cancel out in the reflection. When the increased voltage initiates the phase change process of the VO_2 layer, the higher loss of metallic VO_2 suppresses the formation of the magnetic dipole between two metal layers, resulting in the reduction in emissivity. The white dashed lines in Fig. 3(b) indicate the phase change interface, where the metallic VO_2 region starts from the centerline at a lower voltage of 0.6 V and gradually expands toward the nanorod tips with the increased voltage. At the voltage of $U_0 = 0.9$ V, the VO_2 layer becomes metallic under the full length of the nanowire, causing minimal field enhancement and emissivity. It is worth noting that the tunability of the proposed structure comes from the control of the metallic region geometry beneath the nanorods, instead of delicately maintaining the device temperature at the transition region (see the supplementary material, where the optical response can be largely preserved even if the transition zone is eliminated).

The evolution of the emissivity vs the heating voltage is plotted in Fig. 3(c). The emissivity first slowly decreases at the low voltages, and the slope becomes much steeper at higher voltages. This is attributed to the field distribution of the nanorod resonator, where at high voltages, the VO_2 phase-changed region reaches the high electric field tip regions, as shown in Fig. 3(b). When the voltage increases beyond 0.9 V, the VO_2 phase-changed region covers the whole nanorod, leading to the saturated performance of the emitter. From 0.5 to 0.9 V, the continuous modulation of the emissivity from 0.89 to 0.15 is achieved. The emissivity modulation depth in this work is generally comparable to or even better than the binary structures reported in the literature (see Table S3 of the supplementary material for performances of VO_2 based tunable emitters in the literature). It is worth noting that Fig. 3(c) only focuses on the heating process with the phase change temperature fixed at 345 K, while the hysteresis in VO_2 leads to a lower phase change temperature during the cooling process.[46,54] As a result, the emissivity–voltage

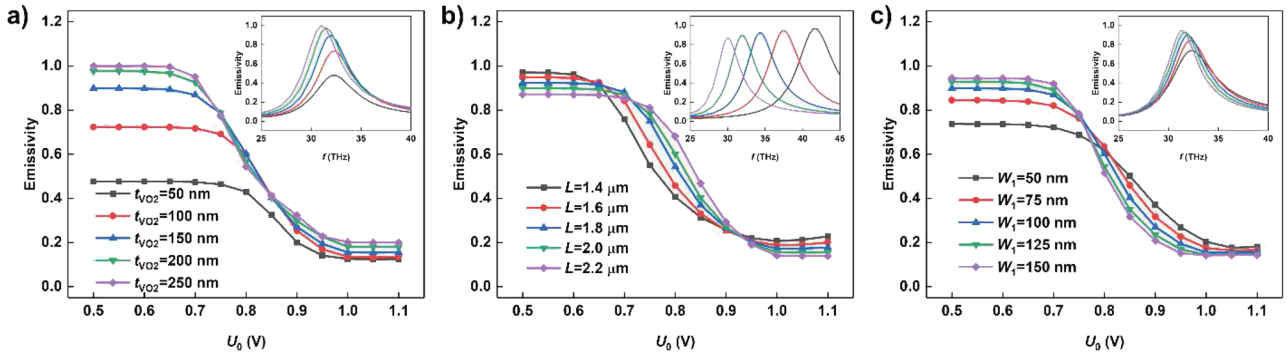

FIG. 4. Simulated emissivity–voltage curves of the nanorod metasurface with respect to (a) VO_2 thickness; (b) nanorod length; and (c) nanorod width, evaluated under the corresponding resonant frequencies at $U_0 = 0$ V. (Insets: emissivity spectrum for the corresponding geometrical parameters at $U_0 = 0$ V).

curve in the cooling process is shifted to lower voltages (see the supplementary material).

The full width half maximum (FWHM) and the frequency shift of the emissivity peak are plotted regarding the heating voltage in Fig. 3(d). The FWHM for different heating voltages is evaluated through curve fitting, which almost remains constant but shows a slightly ascending trend with the heating voltage due to the increase in the ohmic loss inside the metallic VO_2 regions. The emissivity peak shows a slight redshift with the increase in the heating voltage, which can be attributed to the increasing mismatch of impedance with the phase change of the VO_2 layer.

With the incorporation of the centerline Joule heating and phase change of VO_2 layer, the reconfigurable metasurface emitter demonstrates a strong electro-thermo-optical coupling with multiple geometrical and material parameters. As illustrated in Fig. 4, the geometrical parameters with significant and highly entangled thermal and optical couplings, such as the VO_2 layer thickness t_{VO2}, the nanorod length L, and the nanorod width W_1, are investigated. The periodicity also shows some influence on the thermal and optical performances, as discussed in the supplementary material. First, the peak emissivity under the heating voltages from 0.5 to 1.1 V is plotted with five different t_{VO2} in Fig. 4(a), showing a significant influence of the VO_2 thickness on the different maximum emissivity at the resonance, which drops from near 1 to less than 0.5 with the thickness reduced from 250 to 50 nm. However, the emissivity spectrum at zero heating voltage in the inset of Fig. 4(a) indicates that the VO_2 thickness only plays a minor role in tuning the resonant frequency, as the resonance is mainly determined by the dipole resonator of the nanorod. The plot also indicates the influence of the VO_2 thickness on the thermal behavior of the metasurface. Due to the relatively low thermal conductivity of VO_2 layer (~3.6 W/m K for insulating VO_2 and ~6 W/m K for metallic VO_2), a thicker VO_2 layer reduces heat dissipation required for the VO_2 phase transition, resulting in the fast initiation of the phase change. In contrast, a thinner VO_2 film requires a higher heating voltage to reduce the emissivity of the metasurface emitter.

Figure 4(b) shows the spectral performances of the reconfigurable emitter with the gold nanorod lengths from 1.4 to 2.2 μm. It is noted that, in the inset of Fig. 4(b), the emissivity peak frequency for longer nanorods experiences a significant redshift while keeping almost identical maximum emissivity. The emissivity–voltage curve reveals the thermal influence of the nanorod length, where the gold nanorod acts as a heat spreader attached onto the centerline heater. A longer nanorod results in higher heat dissipation capability toward the substrate; thus, the VO_2 phase change initiates at a higher voltage and the emissivity curve shifts to the right. However, the identical substrate structure and nanorod cross section area lead to a similar temperature profile along the nanorod longitudinal direction, resulting in a parallel emissivity–voltage slope for all the five curves toward a high voltage.

The influence of the nanorod width W_1 is analyzed in Fig. 4(c). Unlike the nanorod length, the width is not a major controller of the plasmonic dipole resonator frequency, as the polarization of the nanorod is mainly along the length direction. As a result, the emissivity peak frequency remains around 32 THz for all the widths from 50 to 150 nm, but the maximum emissivity experiences a significant elevation. The thermal influence of the nanorod width can also be found in the emissivity–voltage curve, indicated by a faster decrease in emissivity vs voltage for larger nanorod widths. The larger nanorod cross section area provides a smaller longitudinal thermal resistance, leading to more effective heat spreading and faster expansion of the VO_2 phase-changed region.

In summary, we demonstrate an infrared metasurface emitter with the continuous reconfigurability of emissivity based on the controlled phase change of VO_2 through Joule heating. Using the coupled electro-thermo-optical FEM simulation, we show that the centerline Joule heaters provide precise control of the phase-changed region beneath the nanorods, achieving monotonic and smooth dropping of the metasurface emissivity by more than 50% with the heating voltage increasing from 0.5 to 0.9 V. A series of geometric parameters, including VO_2 layer thickness, nanorod resonator length, and nanorod resonator width, are analyzed to optimize the optical performance. The new metasurface structure extends the binary nature of the PCM modulation to continuous configuration and renders new possibilities toward reconfigurability of nanophotonic devices, including emitters, absorbers, and other metasurface-based devices.

The supplementary material contains the detailed optical and thermal properties in the simulation; simulation setup and VO_2

phase change model; potential fabrication steps for the device; influence of varying periodicity; influence of transition region in the electromagnetic simulation; influence of hysteresis between the heating and cooling processes; and modulation depth compared with literature studies.

The authors acknowledge the Defense Threat Reduction Agency (Grant No. HDTRA1-19-1-0028) and the National Science Foundation (Grant No. CBET-1931964).

AUTHOR DECLARATIONS

Conflict of Interest

The authors have no conflicts to disclose.

Author Contributions

Z.W., L.J., X. Liu, and X. Luo contributed equally to this work.

Zexiao Wang: Data curation (equal); Formal analysis (equal); Investigation (equal); Methodology (equal); Software (equal); Writing – original draft (equal). **Lin Jing**: Data curation (equal); Formal analysis (equal); Investigation (equal); Methodology (equal); Software (equal); Writing – original draft (equal). **Xiu Liu**: Data curation (equal); Formal analysis (equal); Investigation (equal); Methodology (equal); Writing – review & editing (equal). **Xiao Luo**: Data curation (equal); Formal analysis (equal); Investigation (equal); Methodology (equal); Writing – review & editing (equal). **Hyeong Seok Yun**: Formal analysis (equal); Investigation (equal); Software (equal); Validation (equal); Writing – review & editing (equal). **Zhuo Li**: Investigation (equal); Methodology (equal); Validation (equal); Writing – review & editing (equal). **Sheng Shen**: Conceptualization (equal); Funding acquisition (equal); Project administration (equal); Resources (equal); Supervision (equal).

DATA AVAILABILITY

The data that support the findings of this study are available from the corresponding author upon reasonable request.

REFERENCES

[1] D. R. Smith, J. B. Pendry, and M. C. K. Wiltshire, "Metamaterials and negative refractive index," Science **305**(5685), 788–792 (2004).

[2] L. Liu, X. Zhang, M. Kenney, X. Su, N. Xu, C. Ouyang, Y. Shi, J. Han, W. Zhang, and S. Zhang, "Broadband metasurfaces with simultaneous control of phase and amplitude," Adv. Mater. **26**(29), 5031–5036 (2014).

[3] A. Tittl, A. K. U. Michel, M. Schäferling, X. Yin, B. Gholipour, L. Cui, M. Wuttig, T. Taubner, F. Neubrech, and H. Giessen, "A switchable mid-infrared plasmonic perfect absorber with multispectral thermal imaging capability," Adv. Mater. **27**(31), 4597–4603 (2015).

[4] A. Lochbaum, Y. Fedoryshyn, A. Dorodnyy, U. Koch, C. Hafner, and J. Leuthold, "On-chip narrowband thermal emitter for mid-IR optical gas sensing," ACS Photonics **4**(6), 1371–1380 (2017).

[5] A. Lenert, D. M. Bierman, Y. Nam, W. R. Chan, I. Celanović, M. Soljačić, and E. N. Wang, "A nanophotonic solar thermophotovoltaic device," Nat. Nanotechnol. **9**(2), 126–130 (2014).

[6] P. Li, B. Liu, Y. Ni, K. K. Liew, J. Sze, S. Chen, and S. Shen, "Large-scale nanophotonic solar selective absorbers for high-efficiency solar thermal energy conversion," Adv. Mater. **27**(31), 4585–4591 (2015).

[7] O. Yurduseven, D. L. Marks, T. Fromenteze, and D. R. Smith, "Dynamically reconfigurable holographic metasurface aperture for a Mills-Cross monochromatic microwave camera," Opt. Express **26**(5), 5281 (2018).

[8] S. Y. Lee, Y. H. Kim, S. M. Cho, G. H. Kim, T. Y. Kim, H. Ryu, H. N. Kim, H. B. Kang, C. Y. Hwang, and C. S. Hwang, "Holographic image generation with a thin-film resonance caused by chalcogenide phase-change material," Sci. Rep. **7**, 041152 (2017).

[9] L. Li, T. Jun Cui, W. Ji, S. Liu, J. Ding, X. Wan, Y. Bo Li, M. Jiang, C. W. Qiu, and S. Zhang, "Electromagnetic reprogrammable coding-metasurface holograms," Nat. Commun. **8**(1), 197 (2017).

[10] Y. Qu, Q. Li, L. Cai, M. Pan, P. Ghosh, K. Du, and M. Qiu, "Thermal camouflage based on the phase-changing material GST," Light: Sci. Appl. **7**(1), 26 (2018).

[11] N. Lee, T. Kim, J. S. Lim, I. Chang, and H. H. Cho, "Metamaterial-selective emitter for maximizing infrared camouflage performance with energy dissipation," ACS Appl. Mater. Interfaces **11**(23), 21250–21257 (2019).

[12] X. Wan, Q. Zhang, T. Yi Chen, L. Zhang, W. Xu, H. Huang, C. Kun Xiao, Q. Xiao, and T. Jun Cui, "Multichannel direct transmissions of near-field information," Light: Sci. Appl. **8**(1), 60 (2019).

[13] C. X. Huang, J. Zhang, Q. Cheng, and T. J. Cui, "Polarization modulation for wireless communications based on metasurfaces," Adv. Funct. Mater. **31**(36), 2103379 (2021).

[14] J. Li, Z. Li, X. Liu, S. Maslovski, and S. Shen, "Active control of thermal emission by graphene-nanowire coupled plasmonic metasurfaces," Phys. Rev. B **106**(11), 115416 (2022).

[15] Y. Horie, A. Arbabi, E. Arbabi, S. M. Kamali, and A. Faraon, "High-speed, phase-dominant spatial light modulation with silicon-based active resonant antennas," ACS Photonics **5**(5), 1711–1717 (2018).

[16] P. C. Wu, R. A. Pala, G. Kafaie Shirmanesh, W.-H. Cheng, R. Sokhoyan, M. Grajower, M. Z. Alam, D. Lee, and H. A. Atwater, "Dynamic beam steering with all-dielectric electro-optic III–V multiple-quantum-well metasurfaces," Nat. Commun. **10**(1), 3654 (2019).

[17] X. Liu and W. J. Padilla, "Reconfigurable room temperature metamaterial infrared emitter," Optica **4**(4), 430 (2017).

[18] L. Jing, Z. Li, H. Salihoglu, X. Liu, and S. Shen, "Tunable near-field thermal rectifiers by nanostructures," Mater. Today Phys. **29**, 100921 (2022).

[19] Y. Wang, P. Landreman, D. Schoen, K. Okabe, A. Marshall, U. Celano, H. S. P. Wong, J. Park, and M. L. Brongersma, "Electrical tuning of phase-change antennas and metasurfaces," Nat. Nanotechnol. **16**(6), 667–672 (2021).

[20] T. Cao, X. Zhang, W. Dong, L. Lu, X. Zhou, X. Zhuang, J. Deng, X. Cheng, G. Li, and R. E. Simpson, "Tuneable thermal emission using chalcogenide metasurface," Adv. Opt. Mater. **6**(16), 1800169 (2018).

[21] S. Abdollahramezani, O. Hemmatyar, M. Taghinejad, H. Taghinejad, A. Krasnok, A. A. Eftekhar, C. Teichrib, S. Deshmukh, M. A. El-Sayed, E. Pop, M. Wuttig, A. Alù, W. Cai, and A. Adibi, "Electrically driven reprogrammable phase-change metasurface reaching 80% efficiency," Nat. Commun. **13**(1), 1696 (2022).

[22] Y. Zhang, C. Fowler, J. Liang, B. Azhar, M. Y. Shalaginov, S. Deckoff-Jones, S. An, J. B. Chou, C. M. Roberts, V. Liberman, M. Kang, C. Ríos, K. A. Richardson, C. Rivero-Baleine, T. Gu, H. Zhang, and J. Hu, "Electrically reconfigurable non-volatile metasurface using low-loss optical phase-change material," Nat. Nanotechnol. **16**(6), 661–666 (2021).

[23] Z. Xu, Q. Li, K. Du, S. Long, Y. Yang, X. Cao, H. Luo, H. Zhu, P. Ghosh, W. Shen, and M. Qiu, "Spatially resolved dynamically reconfigurable multilevel control of thermal emission," Laser Photonics Rev. **14**(1), 1900162 (2020).

[24] M. C. Sherrott, P. W. C. Hon, K. T. Fountaine, J. C. Garcia, S. M. Ponti, V. W. Brar, L. A. Sweatlock, and H. A. Atwater, "Experimental demonstration of >230° phase modulation in gate-tunable graphene–gold reconfigurable mid-infrared metasurfaces," Nano Lett. **17**(5), 3027–3034 (2017).

[25] V. V. Zolotarev, S. O. Slipchenko, I. S. Shashkin, A. E. Kazakova, V. A. Kriuchkov, and N. A. Pikhtin, "Modulator chip based on semiconductor heterostructures with a surface diffraction grating for laser beam steering," Appl. Opt. **60**(30), 9287 (2021).

[26]Z. Wang, Y. Ma, M. Li, L. Wu, T. Guo, Y. Zheng, Q. Chen, and Y. Fu, "A thermal-switchable metamaterial absorber based on the phase-change material of vanadium dioxide," Nanomaterials **12**(17), 3000 (2022).
[27]R. Sun, P. Zhou, W. Ai, Y. Liu, Y. Li, R. Jiang, W. Li, X. Weng, L. Bi, and L. Deng, "Broadband switching of mid-infrared atmospheric windows by VO_2-based thermal emitter," Opt. Express **27**(8), 011537 (2019).
[28]X. Lu, B. Dong, H. Zhu, Q. Shi, L. Tang, Y. Su, C. Zhang, W. Huang, and Q. Cheng, "Two-channel VO_2 memory meta-device for terahertz waves," Nanomaterials **11**(12), 3409 (2021).
[29]T. Driscoll, H.-T. Kim, B.-G. Chae, B.-J. Kim, Y.-W. Lee, N. M. Jokerst, S. Palit, D. R. Smith, M. Di Ventra, and D. N. Basov, "Memory metamaterials," Science **325**(5947), 1518–1521 (2009).
[30]R. Xu and Y.-S. Lin, "Tunable infrared metamaterial emitter for gas sensing application," Nanomaterials **10**(8), 1442 (2020).
[31]M. U. Pralle, N. Moelders, M. P. McNeal, I. Puscasu, A. C. Greenwald, J. T. Daly, E. A. Johnson, T. George, D. S. Choi, I. El-Kady, and R. Biswas, "Photonic crystal enhanced narrow-band infrared emitters," Appl. Phys. Lett. **81**(25), 4685–4687 (2002).
[32]D. Franklin, S. Modak, A. Vázquez-Guardado, A. Safaei, and D. Chanda, "Covert infrared image encoding through imprinted plasmonic cavities," Light: Sci. Appl. **7**(1), 93 (2018).
[33]C. Kim, Y. Kim, and M. Lee, "Laser-induced tuning and spatial control of the emissivity of phase-changing $Ge_2Sb_2Te_5$ emitter for thermal camouflage," Adv. Mater. Technol. **7**(8), 2101349 (2022).
[34]Z. J. Coppens and J. G. Valentine, "Spatial and temporal modulation of thermal emission," Adv. Mater. **29**(39), 1701275 (2017).
[35]O. Salihoglu, H. B. Uzlu, O. Yakar, S. Aas, O. Balci, N. Kakenov, S. Balci, S. Olcum, S. Süzer, and C. Kocabas, "Graphene-based adaptive thermal camouflage," Nano Lett. **18**(7), 4541–4548 (2018).
[36]X. Liu, L. Jing, X. Luo, B. Yu, S. Du, Z. Wang, H. Kim, Y. Zhong, and S. Shen, "Electrically driven thermal infrared metasurface with narrowband emission," Appl. Phys. Lett. **121**(13), 131703 (2022).
[37]H. Zhu, J. Li, L. Du, L. Shan, P. Li, X. Lu, T. Feng, S. Das, W. Huang, Q. Shi, and L. Zhu, "VO_2-metallic hybrid metasurfaces for agile terahertz wave modulation by phase transition," APL Mater. **10**(3), 031112 (2022).
[38]W. Tang, K. Xu, P. Wang, and X. Li, "Surface roughness and resistivity of Au film on Si-(111) substrate," Microelectron. Eng. **66**(1–4), 445–450 (2003).
[39]D. G. Baranov, Y. Xiao, I. A. Nechepurenko, A. Krasnok, A. Alù, and M. A. Kats, "Nanophotonic engineering of far-field thermal emitters," Nat. Mater. **18**(9), 920–930 (2019).
[40]M. F. Picardi, K. N. Nimje, and G. T. Papadakis, "Dynamic modulation of thermal emission—A Tutorial," J. Appl. Phys. **133**(11), 111101 (2023).
[41]A. Cappella, J.-L. Battaglia, V. Schick, A. Kusiak, A. Lamperti, C. Wiemer, and B. Hay, "High temperature thermal conductivity of amorphous Al_2O_3 thin films grown by low temperature ALD," Adv. Eng. Mater. **15**(11), 1046–1050 (2013).
[42]C. S. Gorham, J. T. Gaskins, G. N. Parsons, M. D. Losego, and P. E. Hopkins, "Density dependence of the room temperature thermal conductivity of atomic layer deposition-grown amorphous alumina (Al_2O_3)," Appl. Phys. Lett. **104**(25), 253107 (2014).
[43]D.-W. Oh, C. Ko, S. Ramanathan, and D.G. Cahill, "Thermal conductivity and dynamic heat capacity across the metal-insulator transition in thin film VO_2," Appl. Phys. Lett. **96**(15), 151906 (2010).
[44]J. Yang, E. Ziade, and A. J. Schmidt, "Uncertainty analysis of thermoreflectance measurements," Rev. Sci. Instrum. **87**(1), 014901 (2016).
[45]G. Hamaoui, N. Horny, C. L. Gomez-Heredia, J. A. Ramirez-Rincon, J. Ordonez-Miranda, C. Champeaux, F. Dumas-Bouchiat, J. J. Alvarado-Gil, Y. Ezzahri, K. Joulain, and M. Chirtoc, "Thermophysical characterisation of VO_2 thin films hysteresis and its application in thermal rectification," Sci. Rep. **9**(1), 8728 (2019).
[46]J. Ordonez-Miranda, Y. Ezzahri, K. Joulain, J. Drevillon, and J. J. Alvarado-Gil, "Modeling of the electrical conductivity, thermal conductivity, and specific heat capacity of VO_2," Phys. Rev. B **98**(7), 075144 (2018).
[47]A. S. Barker, H. W. Verleur, and H. J. Guggenheim, "Infrared optical properties of vanadium dioxide above and below the transition temperature," Phys. Rev. Lett. **17**(26), 1286–1289 (1966).
[48]Y. Yang, S. Basu, and L. Wang, "Radiation-based near-field thermal rectification with phase transition materials," Appl. Phys. Lett. **103**(16), 163101 (2013).
[49]E. D. Palik, *Handbook of Optical Constants of Solids* (Academic Press, 1998).
[50]P. Berini, "Optical beam steering using tunable metasurfaces," ACS Photonics **9**(7), 2204–2218 (2022).
[51]X. Liu, Z. Li, Z. Wang, H. S. Yun, and S. Shen, "Design and analysis of electrothermal metasurfaces," Front. Energy **17**(1), 134–140 (2022).
[52]C. Qu, S. Ma, J. Hao, M. Qiu, X. Li, S. Xiao, Z. Miao, N. Dai, Q. He, S. Sun, and L. Zhou, "Tailor the functionalities of metasurfaces based on a complete phase diagram," Phys. Rev. Lett. **115**(23), 235503 (2015).
[53]A. Pors and S. I. Bozhevolnyi, "Plasmonic metasurfaces for efficient phase control in reflection," Opt. Express **21**(22), 027438 (2013).
[54]Z. Shao, X. Cao, H. Luo, and P. Jin, "Recent progress in the phase-transition mechanism and modulation of vanadium dioxide materials," NPG Asia Mater. **10**(7), 581–605 (2018).